J|A|C|S
ARTICLES
Published on Web 01/23/2007

A Mechanism for Non-stoichiometry in the Lithium Amide/Lithium Imide Hydrogen Storage Reaction

William I. F. David,*[,†,‡] Martin O. Jones,[‡] Duncan H. Gregory,[§] Catherine M. Jewell,[§] Simon R. Johnson,[‡] Allan Walton,[||] and Peter P. Edwards[‡]

Contribution from the ISIS Facility, Rutherford Appleton Laboratory, Chilton, Didcot, Oxon OX11 0QX, U.K., Inorganic Chemistry Laboratory, University of Oxford, South Parks Road, Oxford OX1 3QR, U.K., WestCHEM, Department of Chemistry, University of Glasgow, Glasgow G12 8QQ, U.K., and Department of Metallurgy and Materials, University of Birmingham, Edgbaston, Birmingham B15 2TT, U.K.

Received August 18, 2006; E-mail: bill.david@rl.ac.uk

Abstract: We demonstrate, through structural refinement from synchrotron X-ray diffraction data, that the mechanism of the transformation between lithium amide and lithium imide during hydrogen cycling in the important Li−N−H hydrogen storage system is a bulk reversible reaction that occurs in a non-stoichiometric manner within the cubic anti-fluorite-like Li−N−H structure.

Introduction

One of the most promising lightweight hydrogen storage systems involves hydrogen cycling between lithium nitride, lithium imide, and lithium amide.[1−3] This system undergoes two distinct and reversible hydrogenation steps that can be formally written as

$$Li_3N + H_2 \leftrightarrow Li_2NH + LiH \quad (1)$$

$$Li_2NH + H_2 \leftrightarrow LiNH_2 + LiH \quad (2)$$

These two reaction steps correspond to a total hydrogen storage potential of 10.4 wt %. While this maximum storage capacity has been demonstrated by several groups,[1−6] its practical application is limited since full desorption to Li_3N from Li_2NH (eq 1) requires temperatures greater than 320 °C in dynamic vacuum.[2]

The desorption step from lithium amide to lithium imide (eq 3)

$$LiNH_2 + LiH \rightarrow Li_2NH + H_2 \quad (3)$$

is viewed as a two-stage process. First, lithium amide decomposes to lithium imide and gaseous ammonia which reacts on a short time scale[3,7,8] with lithium hydride. This reaction, the second stage of the process, produces fresh lithium amide with the release of gaseous hydrogen. The reaction pathway has been written as[3,6]

$$2LiNH_2 \rightarrow Li_2NH + NH_3 \quad (4)$$

$$LiH + NH_3 \rightarrow LiNH_2 + H_2 \quad (5)$$

This desorption step (eq 3), with a maximum potential of 6.5 wt %, occurs under more favorable conditions than eq 1 with full conversion of lithium amide and lithium hydride to lithium imide and hydrogen reported to occur under a dynamic vacuum at less than 200 °C.[4]

In this paper, we describe our experimental observations that lead us to conclude that the reversible hydrogenation step (2) and amide decomposition (4) are both bulk reactions that occur through non-stoichiometric processes. We further propose mechanisms for these reactions based on both Li^+ and H^+ migration.

Experimental Section

Lithium nitride (Li_3N) samples were synthesized by the reaction of molten alkaline earth metal−sodium alloys with dried nitrogen at 460 °C. The cleaned lithium metal (Alfa 99+%) was added to molten sodium (Aldrich 99.95%) in an argon filled glove box and then heated in a stainless steel vessel under nitrogen for 48 h. Excess sodium was then removed by vacuum distillation at 460 °C for 24 h. The identity of the product was confirmed as Li_3N by powder X-ray diffraction[9] (data not included here).

† Rutherford Appleton Laboratory.
‡ University of Oxford.
§ University of Glasgow.
|| University of Birmingham.

(1) Chen, P.; Xiong, Z.; Luo, J.; Lin, J.; Tan, K. L. *Nature* **2002**, *420*, 302−304.
(2) Chen, P.; Xiong, Z.; Luo, J.; Lin, J.; Tan, K. L. *J. Phys. Chem. B* **2003**, *107*, 10967−10970.
(3) Hu, Y. H.; Ruckenstein, E. *J. Phys. Chem. A* **2003**, *107*, 9737−9739.
(4) Pinkerton, F. E. *J. Alloys Compd.* **2005**, *400*, 76−82.
(5) Meisner, G. P.; Pinkerton, F. E.; Meyer, M. S.; Balogh, M. P.; Kundrat, M. D. *J. Alloys Compd.* **2005**, *404−406*, 24−26.
(6) Ichikawa, T.; Hanada, N.; Isobe, S.; Leng, H.; Fujii, H. *J. Phys. Chem. B* **2004**, *108*, 7887−7892.
(7) Hino, S.; Ichikawa, T.; Ogita, N.; Udagawa, M.; Fujii, H. *Chem. Commun.* **2005**, 3038−3040.
(8) Isobe, S.; Ichikawa, T.; Hino, S.; Fujii, H. *J. Phys. Chem. B* **2005**, *109*, 14855−14858.
(9) Gregory, D. H.; O'Meara, P. M.; Gordon, A. G.; Siddons, D. J.; Blake, A. J.; Barker, M. G.; Hamor, T. A.; Edwards, P. P. *J. Alloys Compd.* **2001**, *317−318*, 237−244.

10.1021/ja066016s CCC: $37.00

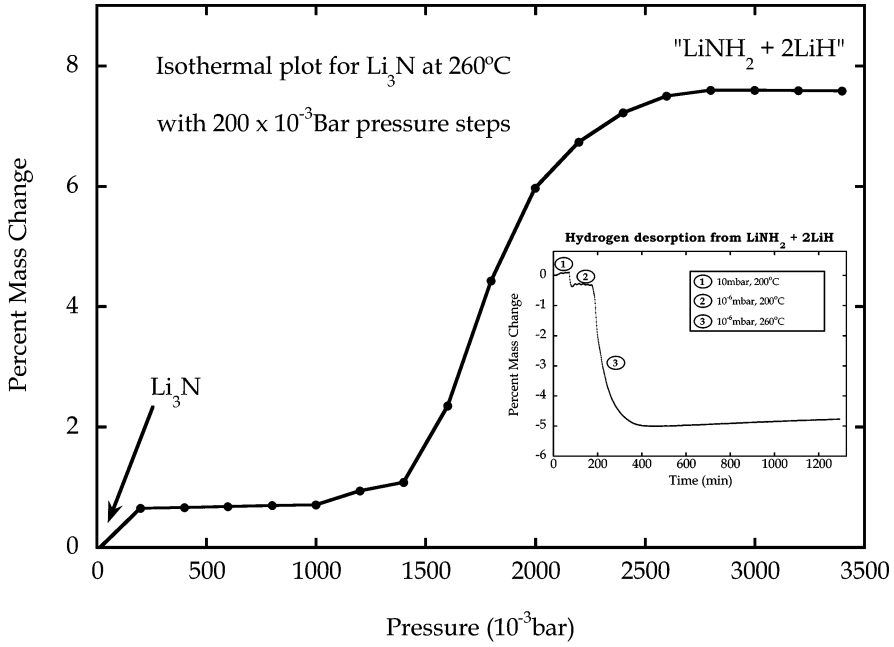

Figure 1. Isothermal hydrogen absorption for a typical sample of Li_3N. The weight gain (7.5 wt %) is equivalent to the absorption of 2.6 hydrogens. The insert shows a typical time-resolved hydrogen desorption, with the weight loss (5.4 wt %) consistent with the formation of Li_2NH and the loss of H_2.

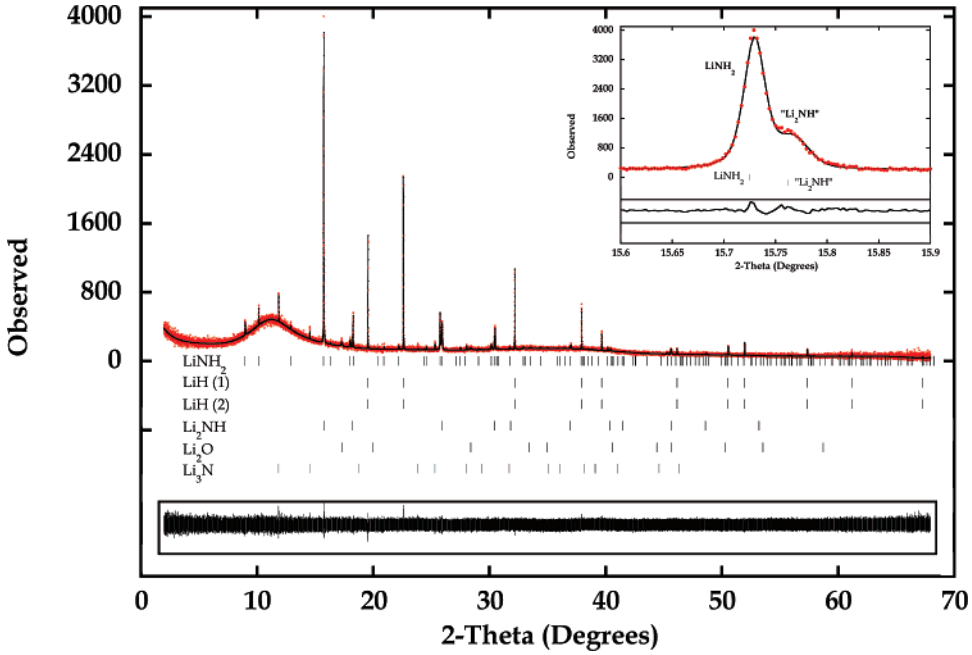

Figure 2. Observed (red dotted line), calculated (solid line), and difference plots ($Y_{obsd} - Y_{calcd}$, solid line in box) for the structure refinement of sample SI from X-ray synchrotron diffraction data collected at $\lambda = 0.8022$ Å and with a step size of 0.003 Å. The Bragg peak positions for $LiNH_2$ and two phases of LiH, Li_3N, Li_2NH, and Li_2O are all shown by the vertical tick marks. The insert highlights the presence of the additional "Li_2NH" component present.

Samples of Li_3N were loaded on a constant pressure thermogravimetric balance (Hiden IGA). Samples were transferred from a glove box to the IGA with an air exposure time of the order of 1 min and underwent a number of hydrogenation/dehydrogenation cycles, each of which consisted of hydrogen absorption at 3 bar and 260 °C and desorption at 10^{-3} bar and 260 °C over a period of 900 min. Synchrotron X-ray diffraction data (0.8022 Å wavelength, step size 0.003 Å) were collected for three samples (denoted as SI, SII, and SIII) on the high-resolution diffractometer ID31 at the ESRF, Grenoble. In sample SI, Li_3N was cycled six times and left in the hydrogenated state (nominally $LiNH_2 + 2LiH$). With SII, Li_3N was cycled once and left in the dehydrogenated state, while, for SIII, Li_3N was cycled six times and left in the dehydrogenated state; both SII and SIII are nominally $Li_2NH + LiH$. A representative hydrogen absorption isotherm for Li_3N is shown in Figure 1, together with a time-resolved desorption (insert) from the resulting $LiNH_2 + 2LiH$.

Results and Discussion

The synchrotron X-ray powder diffraction pattern for sample SI is shown in Figure 2 and is typical of a multicomponent system. The pattern is dominated by $LiNH_2$ and LiH with small amounts of Li_2O and unreacted Li_3N. However, careful examination of the diffraction pattern shows that there is an additional component with a cubic anti-fluorite-like Li−N−H structure that is topologically equivalent to high-temperature disordered

Table 1. Quantitative Analysis of Sample SI (units in moles, normalized to a total of three lithium atoms within the amide−imide−hydride system, with the uncertainty in the figure quoted in brackets)[a]

Li_3N	$LiNH_2$	$Li_{1.15}NH_{1.85}$	LiH	Li_2O
0.08(1)	0.63(1)	0.21(1)	2.17(1)	0.04(1)

[a] The relatively high fraction of LiH and slight departure from ideal 3:1 ratio of Li/N is probably due to ammonia depletion during the cycling process (eq 5).

cubic lithium imide (see Figure 2 insert). The refined lithium stoichiometry in the cubic Li−N−H imide phase in SI is $Li_{1.15}$ which, assuming a charge balanced species, gives an overall stoichiometry of $Li_{1.15}NH_{1.85}$. This is very close to the stoichiometry of lithium amide with almost half the Li tetrahedral sites empty. However, long-range ordering of these vacancies has not occurred, and although the local symmetry is probably tetragonal, the long-range average symmetry is clearly cubic in this phase. The relative molar amounts of the different phases for SI are given in Table 1. Note that the ratio of tetragonal lithium amide plus cubic Li−N−H to lithium hydride is approximately 1:2.6, which is close to the theoretical optimal ratio of 1:2 obtained on the complete hydrogenation of Li_3N as shown in eqs 1 and 2. Comparison of the LiH Bragg peaks between SI and SII/SIII indicates that the SI peaks are broader and shifted to higher *d*-spacings. Initially, it was considered that this corresponded to a single LiH phase. However, the very close coincidence of the lower *d*-spacing component of the Bragg peaks in S1, SII, and SIII suggests the presence of a common LiH phase for all three samples with an additional second phase with higher *d*-spacing in SI. Incorporating this structural model into the Rietveld refinement analysis of the LiH diffraction data suggests a 1:2 ratio of LiH phases with lattice constants 4.083 21(6) Å and 4.084 10(4) Å, respectively (Figure 3). The smaller lattice constant is in close agreement with the refined values obtained from SII and SIII which are 4.083 17(1) Å and 4.083 21(1) Å. While SI may simply have a single broader LiH phase, this analysis suggests that there is a possibility that the LiH formed on hydrogenation of lithium imide from lithium nitride is subtly different from the LiH formed on hydrogenation of lithium amide from lithium imide, although it may be that this is solely due to the difference in applied pressure during the hydrogenation and dehydrogenation segments of the cycling process.

At this point, it is worth highlighting the very close similarities between the tetragonal lithium amide and high-temperature, disordered cubic lithium imide structures. These similarities are not immediately evident on first inspection since cubic lithium imide is usually drawn as a conventional anti-fluorite structure with nitrogen atoms on a face-centered cubic lattice (Figure 4a). Lithium amide, on the other hand, is normally drawn with the Li atoms on the unit cell edges and the nitrogen atoms forming N_4 tetrahedral clusters (Figure 4b). Applying a ($^1/_4$,$^1/_4$,$^1/_4$) shift to the cubic imide structure locates the origin at a Li atom (Figure 4c) and immediately highlights the very close similarities between lithium amide and imide structures. Lithium amide is essentially an ordered (a × a × 2a) superstructure of disordered cubic anti-fluorite lithium imide with half the available Li tetrahedral sites occupied in an ordered manner (Figure 4c). Although the structures are clearly similar, it is also worth noting that while cubic lithium imide is fully three-dimensional in its character, tetragonal lithium amide has a pronounced layered structure because of the conformation of NH_2 groups and the associated ordering of the lithium atoms.

In contrast to SI, samples SII (Figure 5a) and SIII (Figure 5b) show complex microstructural behavior; the significant differences between the diffraction patterns of SI and SII are highlighted in Figure 6. The broad Bragg peaks of the dominant cubic Li−N−H phase, within SII, are highly structured and follow a strain-broadening dependence on diffraction angle, which is indicative of a pronounced stoichiometry variation. Detailed structural modeling of the diffraction data using the profile refinement program TOPAS[10] has allowed the full range of non-stoichiometry present in the sample to be evaluated. The continuous stoichiometry variation of the cubic phase has been modeled by using 11 uniformly varying phases denoted by the formula $Li_{1+x_n}NH_{2-x_n}$, where $x_n = x_{low} + 0.1n(x_{high} - x_{low})$; $n = 0,...,10$. A linear variation in lattice constant behavior is assumed; $a_n = a_{high} + 0.1n(a_{low} - a_{high})$. The refined parameters are the lower (SII = 5.000 13(7) Å, SIII = 4.999 57(6) Å) and upper (SII = 5.079 19(60) Å, SIII = 5.069 92(40) Å) lattice constant bounds, a_{low} and a_{high}, the lower (SII = 0.508(20), SIII = 0.590(10)) and upper (SII = 0.828(12), SIII = 0.850-(60)) stoichiometry bounds, x_{low} and x_{high} (determined from peak positions), and the scale factors associated with each representative phase. Both scale factors and stoichiometry bounds are determined from the Bragg peak areas; there is sufficient peak shape variation between different Bragg peaks to permit the simultaneous refinement of these quantities. Results for SII and SIII are reported in Table 2. Note here that the ratio of non-stoichiometric Li−N−H to lithium hydride is approximately 1:1.14 and 1:1.13 for SII and SIII, respectively, which are close to the theoretical value 1:1.

The stoichiometries for cubic Li−N−H in SII and SIII are represented in Table 3 and range from $Li_{1.08}NH_{1.92}$ to $Li_{1.65}$-$NH_{1.35}$ with a weighted average stoichiometry of $Li_{1.52}NH_{1.48}$ for SII and from $Li_{1.18}NH_{1.82}$ to $Li_{1.70}NH_{1.30}$ with a weighted average stoichiometry of $Li_{1.58}NH_{1.42}$ for SIII. All these stoichiometries retain the cubic anti-fluorite structure reminiscent of lithium imide despite possessing amide-like stoichiometries. The exact composition that corresponds to the transition point between the cubic and tetragonal phases has yet to be identified although we believe that it is likely to be within 10% of the lithium amide stoichiometry.

These observations of continuous non-stoichiometries force a reassessment of the mechanisms of hydrogenation of lithium imide (eq 2) and the decomposition of lithium amide (eq 4). Hence one could modify the mechanism for the hydrogenation of lithium imide originally derived elegantly by Fujii et al. for a stoichiometric system[6−8] to one described by

$$Li_{2-x}NH_{1+x} + \epsilon H_2 \rightarrow Li_{2-(x+\epsilon)}NH_{1+(x+\epsilon)} + \epsilon LiH \quad (6)$$

where non-stoichiometric lithium imide has a lithium-deficient/proton-excess composition. Here, *x* denotes the number of lithium vacancies which, through charge balancing, must equal the number of excess protons. Our diffraction results indicate that the decomposition process for lithium amide is also non-

(10) Coelho, A. TOPAS Academic: 1992−2004.

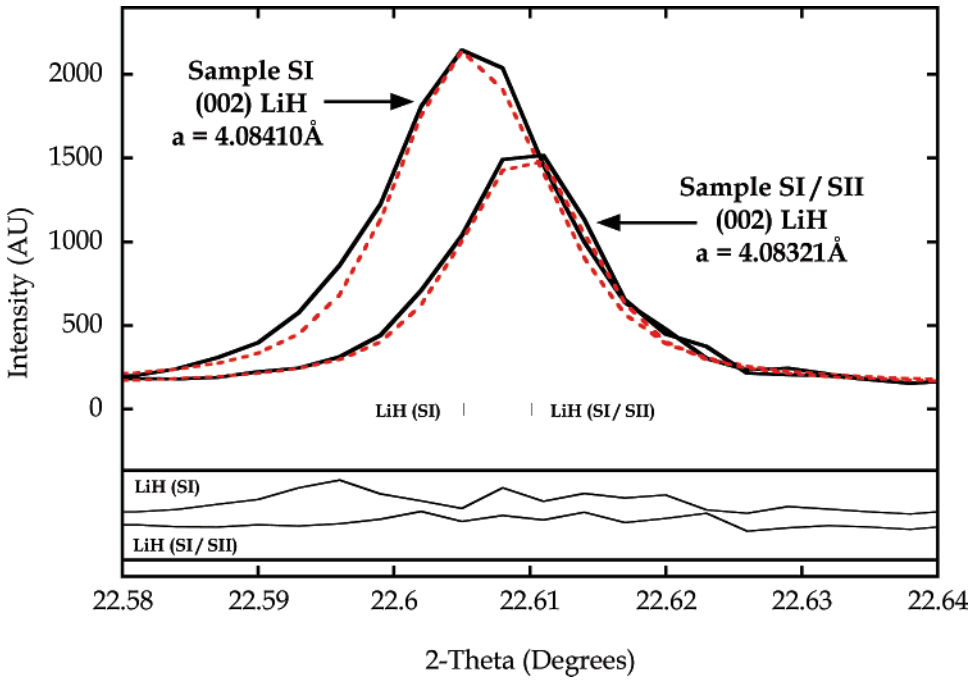

Figure 3. Observed (red dotted line), calculated (solid line), and difference plots ($Y_{obsd} - Y_{calcd}$, solid line in box) for the (002) LiH Bragg peaks for samples SI and SII highlighting the increased breadth and shift to higher *d*-spacing for LiH in sample SI, suggestive of the presence of two differing LiH phases. The tick mark positions for the LiH peaks have been corrected for zero-point error.

stoichiometric and that initially

$$LiNH_2 \rightarrow (1-\epsilon)Li_{1+x}NH_{2-x} + \epsilon NH_3 \qquad (7a)$$

where $(1 + x) = \{1\}/\{(1 - \epsilon)\}$. The decomposition continues in a non-stoichiometric manner so that

$$Li_{1+x}NH_{2-x} \rightarrow (1 - \epsilon)Li_{1+y}NH_{2-y} + \epsilon NH_3 \qquad (7b)$$

(where $(1 + y) = (1 + x)/(1 - \epsilon)$) and the reaction moves continuously from lithium amide to lithium imide stoichiometry. Note that the $(1 - \epsilon)$ term indicates that the amount of solid lithium amide/imide also gradually reduces in this stage of the process. The evolved ammonia rapidly reacts with lithium hydride, forming lithium amide and releasing hydrogen gas; specifically,

$$LiH + \epsilon NH_3 \rightarrow [1-\epsilon(1 + x)]LiH + \epsilon Li_{1+x}NH_{2-x} + \epsilon(1 + x)H_2 \qquad (8)$$

However, given that the reaction of ammonia will occur molecule by molecule at the LiH surface, it is very unlikely that more hydrogen will be produced than ammonia available, and thus, we may conclude that the amide is produced directly from the reaction of ammonia with LiH and therefore

$$LiH + \epsilon NH_3 \rightarrow (1 - \epsilon)LiH + \epsilon LiNH_2 + \epsilon H_2 \qquad (9)$$

Note that this process results in a reduction of the amount of LiH and the generation of a small amount of fresh $LiNH_2$ that exactly balances the loss of non-stoichiometric lithium amide/imide (7b). We thus observe that the production of lithium imide occurs in a gradual, non-stoichiometric manner through the evolution of NH_3 (7a/b) which then reacts with LiH (9) to evolve H_2 and produce a fresh source of $LiNH_2$, which subsequently converts through the proposed non-stoichiometric mechanism to lithium imide.

The observation of variable stoichiometry in the cubic lithium imide structure strongly suggests that the mechanism for the non-stoichiometric absorption and desorption behavior is driven by Li^+ and H^+ mobility within the cubic lithium imide. Consider first the close structural similarities between lithium amide and lithium imide. Figure 4 shows that tetragonal lithium amide may be regarded as an ordered (a × a × 2a) form of cubic lithium imide with the lithium ions in $LiNH_2$ occupying half the possible tetrahedral sites of Li_2NH. Although, we are unable to determine the precise stoichiometry limit of the $LiNH_2$ (a × a × 2a) superstructure, it is clear that a small amount of non-stoichiometry will lead to substantial microstructural defects which results in a crystal structure that appears, on average, to be cubic although the short-range local structure is most probably tetragonal.

Proposed Mechanism for Hydrogen Storage and Release

It is well-established that materials of the fluorite (CaF_2) structure undergo a superionic transition at a temperature that is approximately 80% of the melting point temperature.[11] The superionic conductivity is due to thermally activated disorder in the anionic lattice, which takes the form of short-lived anion Frenkel-defect pairs, with anion diffusion occurring by correlated hopping between existing anion sites in the [100] direction.[11,12]

Similar behavior is also found in materials with the antifluorite structure; here the positions of the cations and anions are reversed so that it is the cation that is the mobile species. Studies

(11) Hayes, W.; Hutchings, M. T. *Ionic Solids at High Temperatures*; Stoneham, A. M., Ed.; World Scientific: 1989.
(12) Gillian, M. J. *Ionic Solids at High Temperatures*; Stoneham, A. M., Ed.; World Scientific: 1989.

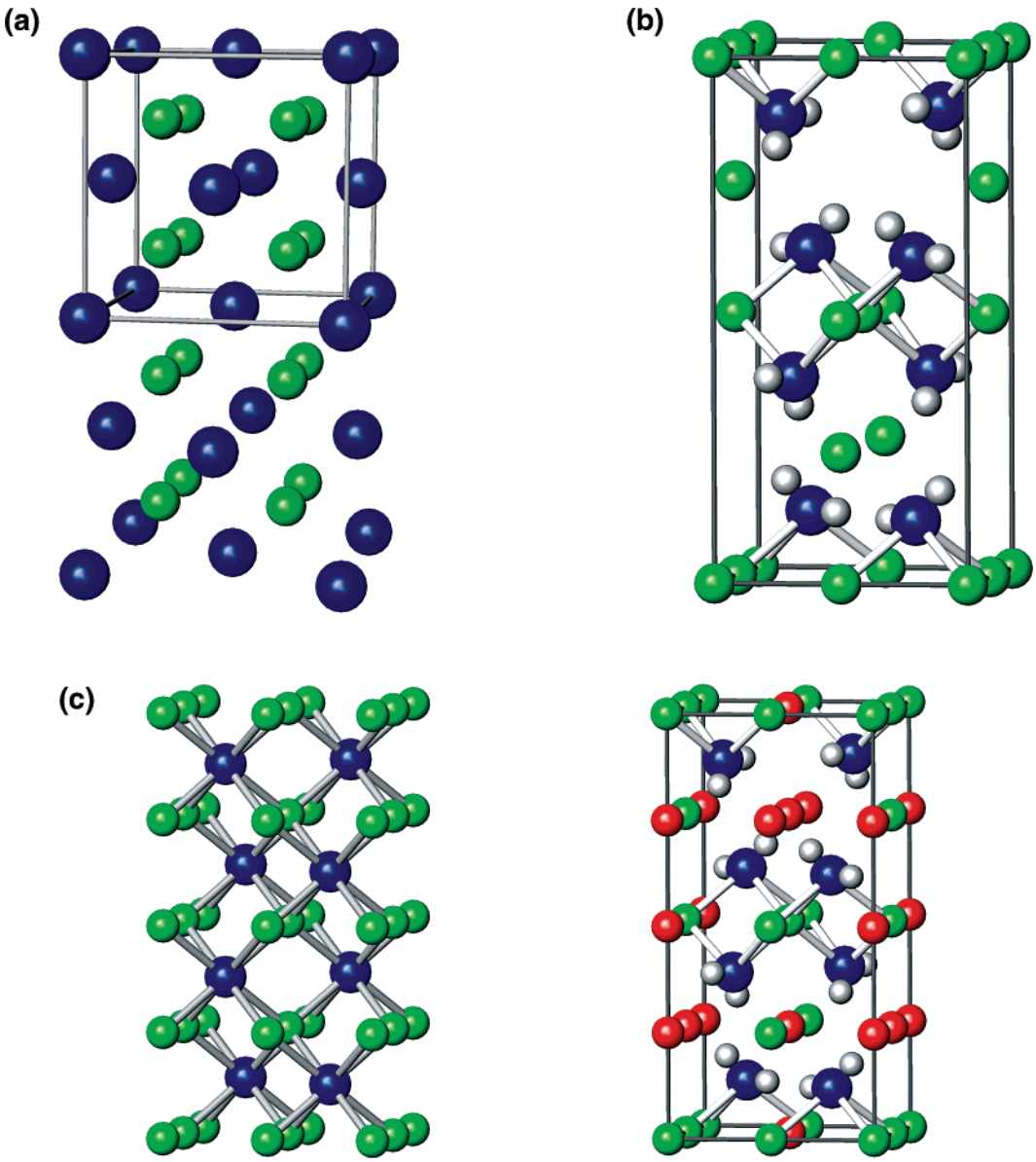

Figure 4. Schematic structures of lithium amide and lithium imide, with nitrogen as blue spheres, lithium as green spheres, and hydrogen as gray spheres. (a) Cubic lithium imide is drawn as a conventional anti-fluorite structure with nitrogen atoms on a face-centered cubic lattice. (b) Tetragonal lithium amide, drawn with the Li atoms on the unit cell edges and the nitrogen atoms forming N_4 tetrahedral clusters. (c) A comparison of cubic lithium imide with the origin shifted by ($^1/_4$,$^1/_4$,$^1/_4$) to locate at a Li atom and tetragonal lithium amide amide represented as an ordered (a × a × 2a) superstructure of cubic antifluorite lithium imide, with the ordered, unoccupied Li tetrahedral sites represented by red spheres, highlighting the very close similarities between the structures.

on lithium oxide (Li_2O), which is topographically equivalent to cubic Li_2NH, confirm this, with Li^+ migration in antifluorite Li_2O structures proceeding by direct tetrahedral to tetrahedral sites hopping along the [100] direction,[13,14] at low temperature, with an additional tetrahedral to octahedral site pathway becoming more favorable at higher temperatures. Indeed, structural studies of Li_2NH by Noritake et al. have indicated that a small number of Li cation vacancies (5%) are present at room temperature.[15−17]

Consequently, in lithium imide—and the structurally similar lithium amide—our diffraction data suggest that a similar ionic mobility exists, especially at the temperature of hydrogenation which approaches 80% of the melting temperature (75% of decomposition temperature for Li_2NH and 70% of the melting temperature of $LiNH_2$). Given this suggestion, and using a short-lived Frenkel defect pair model, we may identify mechanisms for the key processes involved in the decomposition of lithium amide to lithium imide and the resultant production of ammonia.

The principal step in our proposed mechanism is the movement of a lithium cation to an adjacent, vacant, tetrahedral or octahedral site, creating a Frenkel defect pair. Such a process will create two adjacent, unstable, charged species, $[LiLiNH_2]^+$ and $[\square NH_2]^-$, where $\square$ is a formerly Li^+-occupied

(13) Farley, T. W. D.; Hayes, W.; Hull, S.; Hutchings, M. T.; Vrtis, M. *J. Phys. Condens. Mater* **1991**, *3*, 4761−4781.
(14) Hayoun, M.; Meyer, M.; Denieport, A. *Acta Mater.* **2005**, *53*, 2867−2874.
(15) Noritake, T.; Nozaki, H.; Aoki, M.; Towata, S.; Kitahara, G.; Nakamori, Y.; Orimo, S. *J. Alloys Compd.* **2005**, *393*, 264−268.
(16) Balogh, M. P.; Jones, C. Y.; Herbst, J. F.; Hector, L. G.; Kundrat, M. *J. Alloys Compd.* **2006**, *420*, 326−336.
(17) Ohoyama, K.; Nakamori, Y.; Orimo, S.; Yamada, K. *J. Phys. Soc. Jpn.* **2005**, *74*, 483−487.

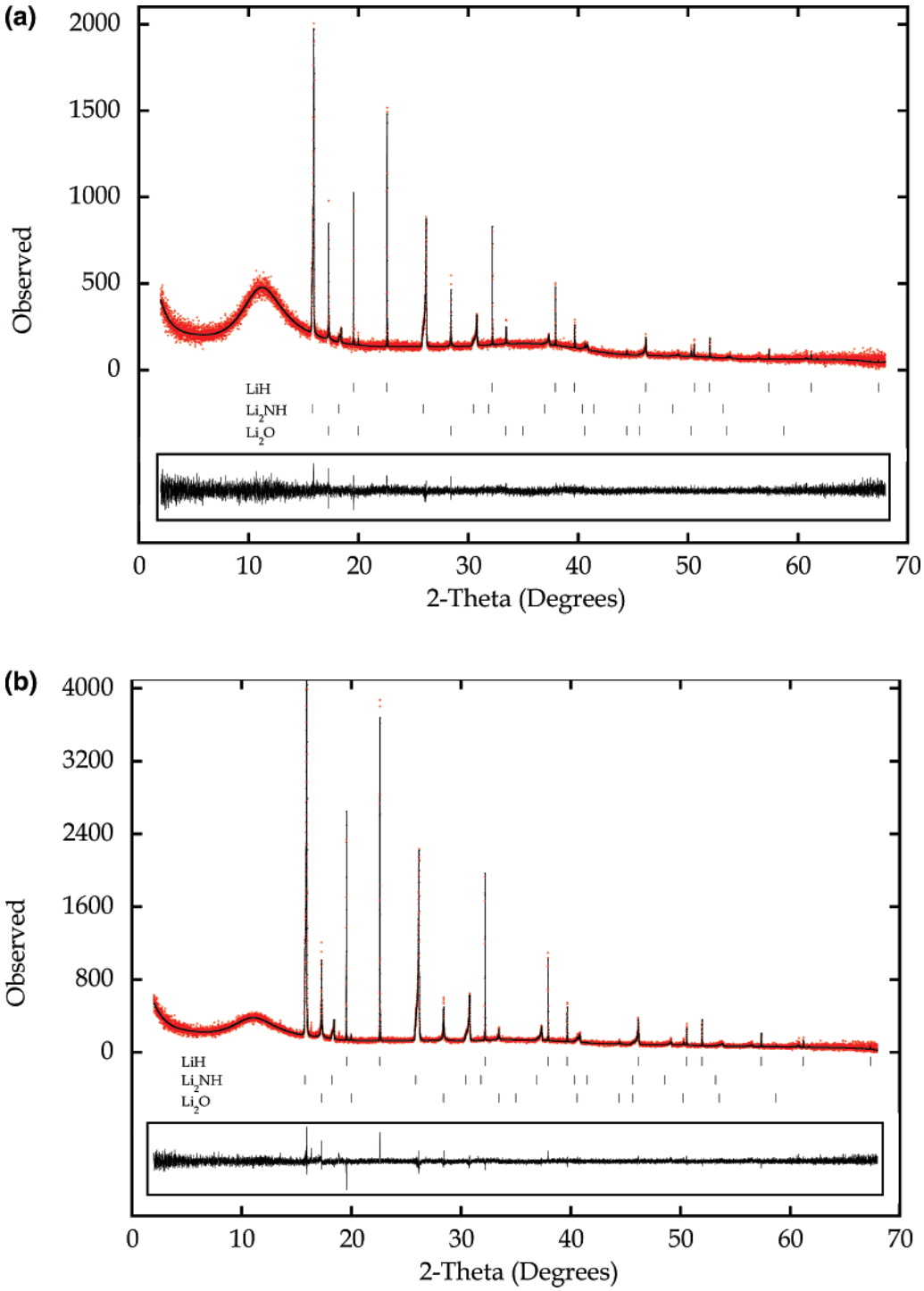

Figure 5. Observed (red dotted line), calculated (solid line), and difference plots ($Y_{obsd} - Y_{calcd}$, solid line in box) for the structure refinement of sample SII (a) and SIII (b) from X-ray synchrotron diffraction data collected at $\lambda = 0.8022$ Å and with a step size of 0.003 Å. The Bragg peak positions for LiH, Li_2NH, and Li_2O are all shown by the vertical tick marks The complex microstructure and two-theta dependent strain broadening in these data can be observed on the low 2-theta sides of the Li_2NH diffraction peaks. For clarity only the tick marks for the dominant Li_2NH phase are shown.

tetrahedral site (eq 10).

$$LiNH_2 + LiNH_2 \leftrightarrow [LiLiNH_2]^+ + [\square NH_2]^- \qquad (10)$$

Charge balance at this atomic level may be restored (i) by the rediffusion of the migratory Li^+ cation back to its original tetrahedral site (recombination of the Frenkel-defect pair), (ii) by a subsequent site hopping of a Li^+ cation without recombination of the pair (eq 11a), or (iii) by the expulsion of a proton from $[LiLiNH_2]^+$ (eq 11b).

$$[LiLiNH_2]^+ \rightarrow LiNH_2 + Li^+ \qquad (11a)$$

$$[LiLiNH_2]^+ \rightarrow Li_2NH + H^+ \qquad (11b)$$

In the latter, this proton will be attracted to the nearby, negatively charged, unoccupied, tetrahedral site of the $[\square NH_2]^-$

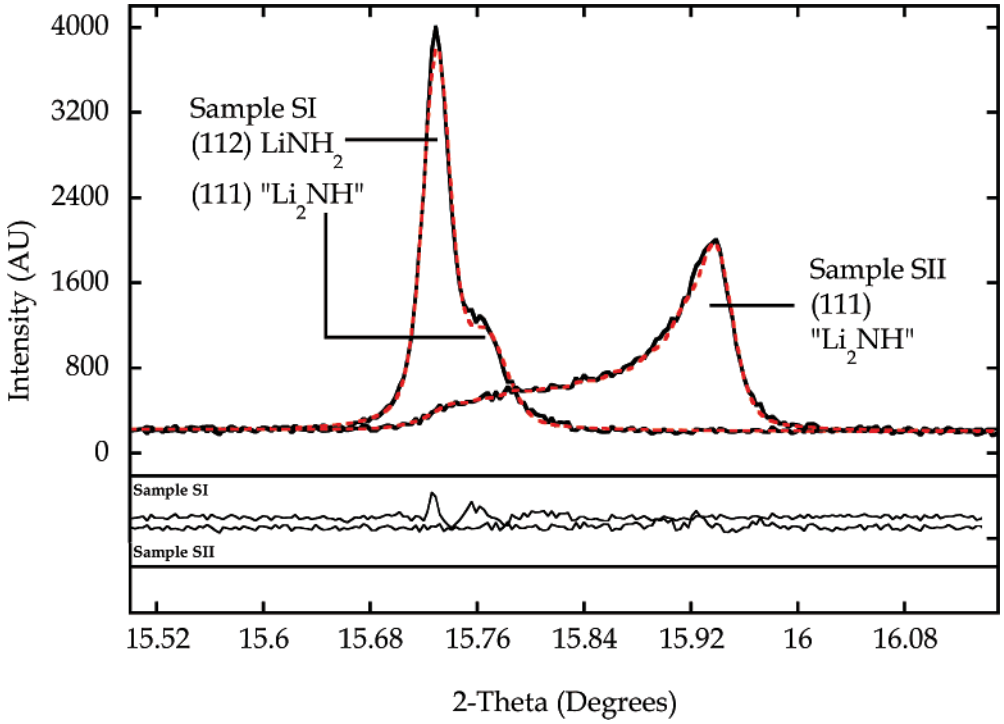

Figure 6. Observed (red dotted line), calculated (solid line), and difference plots ($Y_{obsd} - Y_{calcd}$, solid line in box) for the "Li_2NH" (111) and $LiNH_2$ (112) Bragg diffraction peaks for samples SI and the "Li_2NH" (111) Bragg diffraction peak for SII, highlighting the difference between the simple, multicomponent diffraction peaks observed in SI and the complex microstructure and strain-broadening observed in the diffraction peaks of sample SII.

Table 2. Quantitative Analysis of Samples SII and SIII (units in moles, normalized to a total of three lithium atoms within the amide−imide−hydride system, with the uncertainty in the figure quoted in brackets)

sample	Li_3N	$LiNH_2$	Li–N–H	LiH	Li_2O
SII	0.0	0.0	1.4(1)	1.6(1)	0.2(1)
SIII	0.0	0.0	1.4(1)	1.6(1)	0.3(1)

Table 3. Stoichiometries for Cubic Li−N−H in SII and SIII with the Corresponding Weight Percent for Each Stoichiometry[a]

	SII		SIII	
phase name	stoichiometry	weight percent	stoichiometry	weight percent
Li−N−H−00	$Li_{1.02}NH_{1.98}$	0.0(1)	$Li_{1.18}NH_{1.82}$	0.8(1)
Li−N−H−01	$Li_{1.08}NH_{1.92}$	0.5(1)	$Li_{1.23}NH_{1.77}$	1.3(1)
Li−N−H−02	$Li_{1.14}NH_{1.86}$	2.5(1)	$Li_{1.28}NH_{1.72}$	2.2(1)
Li−N−H−03	$Li_{1.21}NH_{1.79}$	2.7(1)	$Li_{1.34}NH_{1.64}$	2.5(1)
Li−N−H−04	$Li_{1.27}NH_{1.73}$	3.7(1)	$Li_{1.39}NH_{1.61}$	3.2(1)
Li−N−H−05	$Li_{1.34}NH_{1.66}$	3.8(1)	$Li_{1.44}NH_{1.56}$	3.5(1)
Li−N−H−06	$Li_{1.40}NH_{1.60}$	4.5(1)	$Li_{1.49}NH_{1.51}$	4.3(2)
Li−N−H−07	$Li_{1.46}NH_{1.54}$	5.4(2)	$Li_{1.54}NH_{1.46}$	5.0(2)
Li−N−H−08	$Li_{1.53}NH_{1.47}$	7.2(2)	$Li_{1.60}NH_{1.40}$	7.3(2)
Li−N−H−09	$Li_{1.60}NH_{1.40}$	12.3(3)	$Li_{1.65}NH_{1.35}$	12.0(2)
Li−N−H−10	$Li_{1.65}NH_{1.35}$	25.9(4)	$Li_{1.70}NH_{1.30}$	24.8(2)

[a] The stoichiometry is obtained from refined lithium occupancies of each individually modeled cubic Li−N−H phase; uncertainties are in the third decimal place. The weight percents are calculated from individual phase scale factors using TOPAS; the uncertainty in these figures are quoted in brackets.

species, forming an NH_3 adduct (eq 12).

$$[\square NH_2]^- + H^+ \rightarrow NH_3 \qquad (12)$$

When this process occurs within the bulk, the ammonia may form as an ammine adduct in a manner similar to that for the tetrahedral coordination of NH_3 molecules around Li in $Li(NH_3)_4$. Consideration of the $Li(NH_3)_4$ structure indicates that this is a sterically reasonable hypothesis. Tetrahedral coordination of Li is found in $LiNH_2$, Li_2NH, and $Li(NH_3)_4$, and Li−N distances are extremely similar in all three compounds (average Li−N distance is 2.13 Å in $LiNH_2$,[18] 2.1854 Å in Li_2NH,[19] and 2.236 Å in $Li(ND_3)_4$[20]). While the ammonia may subsequently react with another migratory Li^+ cation, to reform lithium amide, ammine adducts will remain trapped within the bulk until natural delamination occurs and the ammonia is released at the surface. Ammonia released in this manner will then either react on a very short time scale with the surface of nearby lithium hydride (formed during the hydrogenation of imide to amide) or escape from the system.

An alternative mechanism for the production of hydrogen from the decomposition of lithium amide in the presence of lithium hydride has been proposed by Chen et al. (eq 2), whereby hydrogen is produced directly from the interaction of LiH and $LiNH_2$ without the production of an ammonia intermediate. Such a mechanism will only be seen to occur where there are small crystallites of $LiNH_2$ and LiH and they are in close (touching) proximity. The sharpness of our diffraction peaks indicates that all our materials coherently diffract and thus have particle sizes in the range of 100 nm or larger. Additionally, our materials have not been mechanically milled to enhance mixing, recognized by Chen as essential, and as such the close proximity necessary for this mechanism will not occur in our materials. Therefore, we believe that the ammonia-mediated mechanism is by far the more likely for our materials.

(18) Milman, V.; Winkler, B. *Z. Kristallogr.* **2001**, *216*, 99−104.
(19) Juza, R.; Opp, K. *Z. Anorg. Allg. Chem.* **1951**, *266*, 325−330.
(20) Young, V. G., Jr.; Glaunsinger, W. S.; Von Dreele, R. B. *J. Am. Chem. Soc.* **1989**, *111*, 9260−9261.

For the hydrogenation of lithium imide it is apparent that the NH^{2-} unit of lithium imide interacts with protonic hydrogen to form NH_2^-, a process accompanied by the formation of lithium hydride.

We believe that Li^+ mobility is also at the basis of the mechanism of hydrogenation; the Li^+ ions migrate cooperatively through the cation vacancies. In this mechanism, surface or migratory Li^+ interacts with the applied H_2, forming LiH and protonic hydrogen (eqs 13 and 14).

$$Li_2NH \rightarrow [\square LiNH]^- + Li^+ \quad (13)$$

$$Li^+ + H_2 \rightarrow LiH + H^+ \quad (14)$$

The protonic hydrogen produced will be attracted toward the negatively charged region surrounding the vacant Li^+ tetrahedral site and will bond with a nearby NH^{2-} group to form $(NH_2)^-$ (eq 15).

$$H^+ + [\square LiNH]^- \rightarrow [\square LiNH_2] \quad (15)$$

It is possible that hydrogen molecules react only with surface Li^+ cations, forming LiH and protonic hydrogen, which is then free to migrate into the bulk imide, and complete the hydrogenation (eq 14), and in this case lithium ion migration plays little or no part in the hydrogenation process.

From the above discussion, we draw the conlcusion that both the lithium amide/lithium imide decomposition and hydrogenation processes are dependent on the migration of Li^+ and H^+ ions. The non-stoichiometry observed in lithium imide is a direct result of this ionic mobility.

Lithium nitride [Li_3N] has a high, anisotropic, lithium ion conductivity[21−23] because of lithium ion defects in the Li_2N layers;[24] the highest conductivity occurs within the plane perpendicular to the hexagonal *c*-axis. Hydrogen doping in Li_3N has been shown to cause enhanced ionic conductivity though the creation of an impurity vacancy complex, consisting of NH^{2-} and a lithium vacancy,[25] with the most pronounced increase in conductivity associated with the planes perpendicular to the *c*-axis.[25,26] Thus, the hydrogenation process of Li_3N occurs because of mobile Li^+ cations within the lithium deficient Li_2N layers. Li^+ mobility is thus a key factor in both stages eqs 1 and 2 of hydrogen cycling in the $Li_3N-Li_2NH-LiNH_2$ system. Increasing the Li^+ mobility and/or disorder[27−29] is therefore likely to improve the hydrogen cycling in this and related Li-based systems.

Concluding Remarks

From a detailed analysis of high-resolution synchrotron x-ray diffraction data for the lithium amide−lithium imide hydrogen storage system, we are able to propose a mechanism for hydrogen storage and release. The results and models outlined here may further assist in "tailoring" specific performance properties for the hydrogen storage materials formed from the light elements of the periodic table.

Acknowledgment. The authors wish to acknowledge the financial support of the EPSRC SUPERGEN program and the European Synchrotron Radiation Facility. We further wish to acknowledge Dr. Andy Fitch and Mr. Philip Chater for their invaluable help with the collection of the diffraction data.

Supporting Information Available: Crystallographic information for refined phases. Figures of refined data for samples SII and SII with all tick marks plotted. This material is available free of charge via the Internet at http://pubs.acs.org.

JA066016S

(21) von Alpen, U.; Rabenau, A. Talat, G. H. *Appl. Phys. Lett.* **1976**, *30*, 621−623.
(22) von Alpen, U. *J. Solid State Chem.* **1979**, *29*, 379−393.
(23) Bell, M. F.; Breitschwerdt, A.; von Alpen, U. *Mater. Res. Bull.* **1981**, *16*, 267−272.
(24) Schulz, H.; Thiemann, K. H. *Acta. Crystallogr.* **1979**, *A35*, 309−314.
(25) Wahl, J. *Solid State Commun.* **1979**, *29*, 485−490.
(26) Hooper, A.; Lapp, T.; Skaarup, S. *Mater. Res. Bull.* **1979**, *14*, 1617−1622.
(27) Gregory, D. H.; O'Meara, P. M.; Gordon, A. G.; Hodges, J. P.; Short, S.; Jorgensen, J. D. *Chem. Mater.* **2002**, *14*, 2063−2070.
(28) Gordon, A. G.; Gregory, D. H.; Blake, A. J.; Weston, D. P.; Jones, M. O. *Int. J. Inorg. Mater.* **2001**, *3* (7), 973−981.
(29) Stoeva, Z.; Smith, R. I.; Gregory, D. H. *Chem. Mater.* **2006**, *18*, 313−320.